Composites Part C: Open Access 16 (2025) 100576

Contents lists available at ScienceDirect

Composites Part C: Open Access

journal homepage: www.sciencedirect.com/journal/composites-part-c-open-access

# High elastic modulus GFRP rebar: A guide to manufacture and design of the influencing parameters

Omar Alajarmeh [a,*], Allan Manalo [a], Dmitry Yatsenko [b]

[a] Centre for Future Materials, University of Southern Queensland, Toowoomba 4350, QLD Australia
[b] Beyond Materials Group Pty Ltd, Brisbane 4129, QLD Australia

ARTICLE INFO

*Keywords:*
Pultrusion
GFRP bars
Curing
Fibre volume fraction

ABSTRACT

Glass fibre reinforced polymer (GFRP) bars are increasingly used as internal reinforcement to concrete infrastructures exposed to harsh environment. A wide range of GFRP bars are commercially available but with high discrepancy in properties due to the inconsistent selection of the manufacturing and design parameters. In contrast to steel bars, producing structural GFRP bars requires a bigger actual than nominal bar diameter claiming higher modulus of elasticity. For the first time, this study reviews the current practice of designing the GFRP bar diameter and reasons behind the discrepancy (lower-upper bound of allowable diameter). It also describes the critical manufacturing parameters through pultrusion process. Moreover, it provides a practical demonstration on systematic design and manufacturing procedures of new GFRP bars both theoretically and experimentally. The guidance provided in this study will be valuable to GFRP manufacturers in consistently producing high modulus GFRP bars (Grade III) without varying much from the nominal diameter.

## 1. Introduction

Corrosion of steel bars in reinforced concrete structures is one of the most serious issues confronting the construction and building industry. The aggressive environmental conditions cause the steel to corrode leading to concrete cracking, spalling, and delamination, reducing the service life of the structure. The yearly cost of corrosion worldwide exceeds US$1.8 trillion owing to structure repair and downtime, which equates to 3 % to 4 % of industrialised countries' gross domestic product. Furthermore, high weight to strength ratio continues to be a key concern in the field of civil engineering, such as concrete constructions, anchoring, structural repair, and rehabilitation. A non-corrosive and high strength composite material, such as glass fibre reinforced polymer (GFRP) bar, has proven to be an effective alternative to steel bar for ensuring the long-term performance and the resilience of concrete structures.

GFRP bars are manufactured through a pultrusion process where the glass filaments impregnated by a polymeric resin are heated within a curing die to produce high quality, fully cured, and round solid bars. These bars are then either surface profiled or sand coated for utilisation as internal reinforcement for different concrete members such as beams [1–3], columns [4–6], and decking [7,8]. Despite the available literature on general pultruded FRP composites manufacturing using closed heating die, GFRP bars are commonly manufactured using open heating tunnel. This manufacturing process uses a die to properly cure composite reinforcing bars at high speed and allow for the development of various outer surface patterns including sand coated, helically wound ribs and surface grooves. These surface profiles ensure sufficient bond of GFRP bars with the surrounding concrete. Nevertheless, GFRP bar manufacturing process has not been discussed yet in the literature. To the authors knowledge, no reports are available analysing the design and manufacturing processes despite these parameters are critical in achieving high quality GFRP bars. This study together with the review of current industrial practice is therefore useful in shedding light on these aspects and in designing GFRP bars complaint with national and international material standards.

An overview of the materials currently being used in manufacturing GFRP bars is presented in this study. Moreover, the recommendations of codes and specifications for compliant GFRP bars having physical and mechanical properties suitable as internal reinforcements in concrete structures are evaluated. This information is then analysed to establish a systematic procedure for the theoretical design of high quality GFRP bars. The challenges being faced in open die GFRP bar manufacturing are then identified. The systematic approach of manufacturing high

* Corresponding author.
*E-mail address:* omar.alajarmeh@unisq.edu.au (O. Alajarmeh).

https://doi.org/10.1016/j.jcomc.2025.100576

Available online 27 February 2025

quality GFRP bars was presented begins by examining the resin curing properties with useful tips prior running actual pultrusion trial. Furthermore, a manufacturing trial of GFRP bars with various diameters was conducted in a commercial production line. This includes monitoring the cure kinetics of the resin and evaluating a suite of physical, thermal, and mechanical properties to validate the developed theoretical design approach. The findings of this study will serve as a comprehensive guide for GFRP bar manufacturers, addressing uncertainties surrounding current industrial practices in their development. From a manufacturing perspective, it opens new opportunities to implement developments including the adoption of new resin systems for pultrusion and controlling the production rates including heating temperature and line speed.

## 2. Materials selection

GFRP bars are being manufactured using glass fibres and thermoset resin. The selection of these constituent materials directly affects the physical and mechanical properties, durability performance, and cost of the final product. It should be mentioned that fibres identify the physical and mechanical properties of the GFRP bars, while the resin contributes to their durability. Wide range of glass fibre types are commercially available, as shown in Table 1. However, electrical and corrosion resistant (ECR) glass fibre is the most affordable option for manufacturers due to its high elastic modulus and relatively low cost compared to other types of high performing fibres. It should be highlighted that the properties of the glass fibres determine majorly the elastic modulus and strength of the GFRP bars as the fibre content by weight should be >80 % to achieve high elastic modulus bars.

The resin type, on the other hand, is no less important than the fibres as it bonds the filament together and transfers the internal stresses uniformly. Resin also protects the GFRP bars from the surrounding environment, increasing their durability. Table 2 summarises the common types of resin system used for pultrusion process and comparison of their relative affordability for the manufacturing of GFRP bars. It is to be noted that polyester resin is not recommended for GFRP bars manufacturing due to durability issues [1]. In contrast, according to Table 2, both epoxy and vinyl ester resins are preferable for pultrusion due to their high mechanical and durability properties. Nevertheless, epoxy resin has more credits when using open mold pultrusion manufacturing as it has low shrinkage (less cracking vulnerability after curing) and less odor (volatiles) which contributes to the safety at the manufacturing facility [9,10].

## 3. Design and manufacture of a GFRP bar

### 3.1. Allowable bar size according to the current practice and recommendations

Material specifications for fibre-reinforced polymer bars such as CSA S807–19 [14] and ASTM D7957–22 [15] reported the allowable size range of the GFRP bars that should acquire minimum physical and mechanical properties. It is worth highlighting a comprehensive review on the buildup of these specifications was discussed by Manalo et al.

**Table 2**
Recommended resin types for pultrusion manufacturing [11–13].

| | | Resin type | | |
|---|---|---|---|---|
| | | **Polyester** | **Epoxy** | **Vinyl ester** |
| **Mechanical** | **Tensile Strength (MPa)** | 45–91 | 55–95 | 73–81 |
| | **Tensile Modulus (GPa)** | 2.1–3.45 | 2.75–4.1 | 3–3.35 |
| | **Specific Gravity (gm/cm$^3$)** | 1.1–1.4 | 1.2–1.3 | 1.1–1.3 |
| | **Cure Shrinkage (%)** | 5–12 | 1–5 | 5.4–10.3 |
| **Physical** | **Moisture resistance** | Moderate | High | High |
| | **Odor** | Low | Low | High |
| | **Viscosity** | Low | High | Moderate |
| | **Shrinkage** | High | Low | Moderate/high |
| | **Cost** | Low | Moderate | Moderate/high |

[16]. It can be noticed in Fig. 1a that CSA S807–19 recommends a nominal diameter with a systematic margin compared to the actual bigger and smaller allowable bar diameter by +20 % and −5 % in cross-sectional area, respectively. The Australian material specification for GFRP bars (AS5204–23 [17]) recommends the same cross-sectional area margin as specified in CSA S807–19. On the other hand, ASTM D7957–22 (Fig. 1b) recommends variable margin of the nominal bar diameter compared to the bigger and smaller allowable actual bar diameter based on the industrial practice. Compared to the consistent margin suggested by CSA S807–19, ASTM D7957 reveals a lower margin while the bar diameters increase. This margin on the bar size affects both stiffness and strength as reflected in low minimum requirements for bigger GFRP bars (especially beyond 22 mm bar diameter) in the ASTM D7957. Thus, Fig. 1 shows the consistency that CSA S807 can offer regarding GFRP bar size regulations.

### 3.2. Design the amount of the constituent materials

Designing the fibre-to-resin ratio is essential to achieve the target tensile strength (σ) and elastic modulus ($E$) in GFRP bars. Therefore, Eqs. (1) and 2 are used to empirically design the desired modulus and strength of a GFRP bar, respectively, based on the modulus and strength of the fibres and resin. For design purposes, Fig. 2 shows the effect of the fibre volume fraction ($V_f$) on both modulus and strength of the GFRP bars. In Fig. 2, for instance, epoxy resin was selected with a modulus ($E_m$) of 3 GPa and strength ($\sigma_m$) of 75 MPa, while the ECR glass fibres have a modulus ($E_f$) of 80.3 GPa and strength ($\sigma_f$) of 3420 MPa. It should be mentioned that Eqs. (1) and 2 are used to calculate the modulus and tensile strength of a GFRP bar, respectively.

$$E = E_f(V_f) + E_m(1 - V_f) \quad (1)$$

$$\sigma = \sigma_f(V_f) + \sigma_m(1 - V_f) \quad (2)$$

According to Fig. 2, it can be observed that producing structural GFRP bars (considered as Grade III bars with an E of at least 60 GPa) requires a $V_f$ of >70 % (around 85 % fibre content in weight). This volume

**Table 1**
Available glass fibre types in the market [11].

| | Glass fibre type/grade | | | | | | | |
|---|---|---|---|---|---|---|---|---|
| | **A** | **C** | **D** | **E** | **ECR** | **AR** | **R** | **S-2** |
| **Density (g/cm3)** | 2.44 | 2.52 | 2.14 | 2.58 | 2.72 | 2.7 | 2.54 | 2.46 |
| **Tensile strength (MPa)** | 3310 | 3310 | 2415 | 3445 | 3445 | 3241 | 4135 | 4890 |
| **Tensile modulus (GPa)** | 68.9 | 68.9 | 51.7 | 72.3 | 80.3 | 73.1 | 85.5 | 86.9 |
| **Elongation (%)** | 4.8 | 4.8 | 4.6 | 4.8 | 4.8 | 4.4 | 4.8 | 5.7 |
| *Cost | N/A | M | N/A | L | L | M | M | H |

* N/A: Not available; L: Low; M: Moderate; H: High.

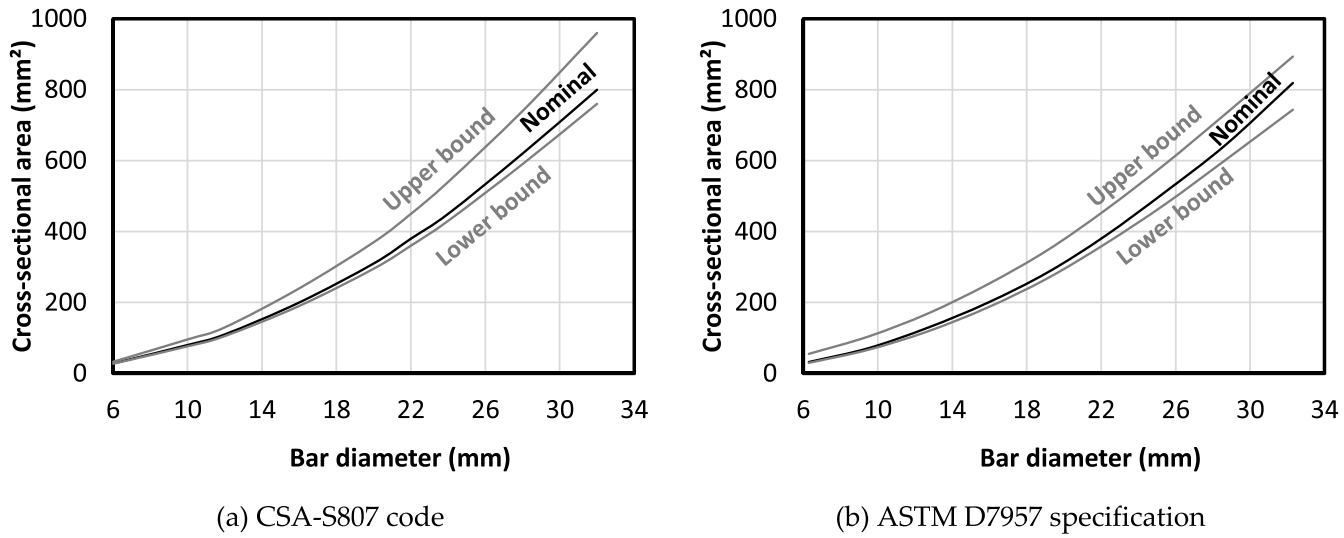


**Fig. 1.** Upper and lower bound of the GFRP bar size.

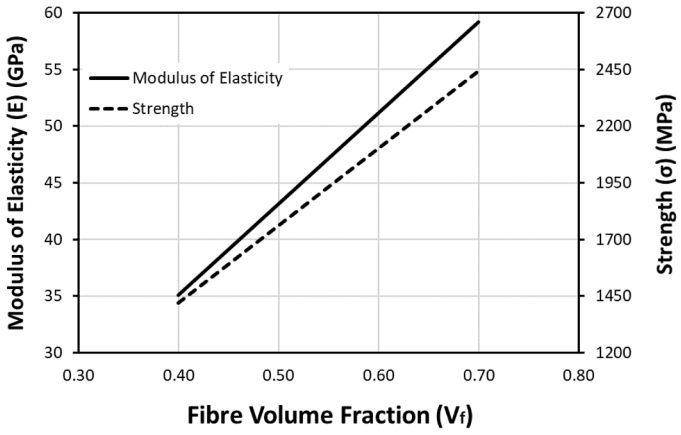


**Fig. 2.** Influence of $V_f$ on the elastic modulus and strength of a GFRP bar.

percentage of fibres is very difficult to achieve when dealing with actual GFRP bar diameter. This $V_f$ percentage requires careful manufacturing process with a high possibility to get dry glass fibre and low transverse mechanical properties due to the low resin content. Therefore, the frequent practice by the industry (which is adopted by the material specifications CSA S807–19 [14] and ASTM D7957–22 [15]and the design codes CSA S806–19 [18] and ACI 440–22 [19]) is to claim lesser nominal diameter compared to the actual one with however a specified range (reflected in Fig. 1). This will increase both modulus and strength of a GFRP bar. For example, an open mold pultrusion process can feasibly achieve $V_f$ of 60 %, which results in $E$ of 49.3 GPa and σ of 2127 MPa (based on the previous given material properties) and considering the actual bar diameter. However, the GFRP bars with this E value are not acceptable for structural applications as this falls within Grade I (bars with E between 40 GPa and 50 GPa) based on CSA S807 and ASTM D7957–22. Thus, making this bar acceptable as Grade III requires claiming lesser bar diameter to the limit that achieves the target E value following the upper and lower bound shown in Fig. 1. Thus, claiming E of 60 GPa out of the 49.3 GPa requires reducing the nominal area of the GFRP bars by 17.8 % compared to the actual area (within the allowable range as seen in Fig. 1). This issue was highlighted by Manalo et al. [16] where the study found that all bars used in Australia are oversized by up to 62 % compared to the actual area. This finding negatively affects the structural design as it does not account for this significant increase in the diameter. Therefore, it is recommended to rely on $V_f$ (for example >65 %) to achieve higher properties making the actual bar diameter closer to the nominal one and leading to more material savings (resin and fibres). Nevertheless, assuring good wettability for the glass fibres by the resin should be carefully considered.

### 3.3. Manufacturing challenges

Open mold pultrusion process is mostly used for manufacturing GFRP bars as it provides an assurance of achieving good quality products. This process requires setting up a well-controlled manufacturing environment including proper fibre guide to prevent fibre tingling (Fig. 3a), squeezers to get rid of the excess amount of resin (Fig. 3b), compatible die with the amount of fibres to form the rounded shape of the bar (Fig. 3c), wound thread to maintain the bar shape and a second step to reduce the amount of extra resin (Fig. 3d), apply sand coating -applicable to sand coated GFRP bars- (Fig. 3e), and proper heat energy to initiate the curing reaction in correlation to the line speed (Fig. 3f). Controlling these parameters results in producing high quality and consistent GFRP bar size.

### 3.4. Resin curing before and during the manufacturing

Resin curing behaviour is crucial in the pultrusion process to optimise the manufacturing line speed and to ensure the highest degree of cure. Therefore, it is essential to raise enough energy required to kick off the curing reaction of the resin. Therefore, the resin curing characteristics should be tested and analysed before the pultrusion trials. The dielectric scanning calorimeter (DSC) test provides the required information about the curing behaviour of the resin including the heat flow, curing rate, and the minimum degree of temperature to kick off the curing reaction. Thermocouple sensors are normally embedded within the real manufacturing line (which is very limited in the literature [20]) to validate the curing properties. This also allows monitoring the temperature profile during the manufacturing process provided useful information on the required line speed to obtain the curing reaction within the pultrusion die. In the next section, these steps and other proposed ones are discussed in detail on a real manufacturing trial of a range of GFRP bar diameters.


**Fig. 3.** Open mould pultrusion manufacturing process of GFRP bars.

## 4. Trial manufacturing of a range of GFRP bars: Industrial case study

### 4.1. Design of the bar size and related mechanical properties

#### 4.1.1. Calculating the number of glass fibre yarns

Deciding the amount of glass fibre yarns requires knowing the maximum achievable $V_f$ in the manufacturing process to achieve the target strength and modulus of elasticity based on the nominal diameter. For example, if the maximum achievable $V_f$ is 65 %, then the modulus of elasticity of the GFRP bar will be 53 GPa (based on $E_f$ of 80 GPa and $E_m$ of 3 GPa) (Eqns. (1) and 2). Therefore, claiming GFRP bar with 60 GPa requires increasing the actual bar area by 13.2 % (= 60 GPa/53 GPa) which is 6.4 % increase in actual diameter. After determining the actual area, the number of glass fibre yarns is calculated based on Eq. (3). Corresponding to the given material properties previously, the number of yarns (with a density ($\rho_f$) of 2620 kg/m$^3$ and yarn tex of 4800 g/km) required to manufacture a GFRP bar with a nominal diameter of 16 mm (199 mm$^2$) is calculated by measuring the actual area (1.132 × 199 = 225.3 mm$^2$) and then apply the given information to Eq. (3) to give an answer of 79.9 ≈ 80 yarns. This number of yarns will ensure achieving a modulus of 60 GPa for a 16 mm GFRP bar nominal diameter. Applying the same equation, 30 yarns and 52 yarns were required to fabricate Grade III bars with diameters of 10 mm and 12 mm, respectively.

$$Number\ of\ yarns = \frac{V_f \times \rho_f(kg/m^3) \times A_{actual}}{yarn\ tex} \quad (3)$$

#### 4.1.2. Design of the metallic forming die

Three GFRP bar diameters were selected to design and pultrude from the beginning of manufacturing. It should be highlighted that the bar diameters were 10 mm, 12 mm and 16 mm representing the mostly used bar diameter in the Australian market [16]. Before quantifying the amount of glass fibre, the metallic forming die (as mentioned in Fig. 3) is responsible to forming the final cross section of the GFRP bar which should be designed based on the maximum allowable actual diameter

for each bar diameter. Thus, Table 3 shows the actual metallic forming die size of the selected bar diameter (same as the maximum allowable bar diameter). It should be highlighted that the acronym M10 in Table 3 means a GFRP bar with a nominal diameter of 10 mm.

The rate of increase in the actual-to-nominal diameter decreases with the increase in the bar diameter. This is attributed to the increase in the friction between the fibre yarns as their amount increases owing to the sizing effect (filament coating) [21]. This means that the actual larger bar diameter has less ability to increase in actual diameter (considering a certain fibre volume fraction ratio). The reasons behind desiring less strength properties for the larger bar diameters by CSA S807 and ACI 440 codes. This issue would be mitigated using close moulding manufacturing process allowing higher compaction to accommodate more fibres but with significantly higher pulling force and lower speed for larger GFRP bar diameters.

### 4.2. Resin cure monitoring and pultrusion process

Resin was tested and analysed in neat form and during the pultrusion process to understand its curing behaviour including heat flow, kick-off temperature and exotherm temperature. It should be highlighted that the resin used in these trials was bisphenol-based epoxy (Part A and B) with initiator (Part C) supplied by ATL Composites, Australia. Small-scale specimens (around 15 mg) were prepared and tested using dielectric scanning calorimeter (DSC) in accordance with ASTM E1356. In addition, a larger quantity of resin (around 50 *g*) in aluminum pans was tested in vacuum oven environment under isothermal heating conditions to obtain more representative results on the reaction rate and exotherm temperature. This method allows inserting of dielectric analysis (DEA) sensors (115L IDEX from NETZSCH-Gerätebau GmbH, Germany) and thermocouples. It should be mentioned that Dielectric Analyser Ionic 288 was used to collect data at frequency of 1 Hz. This method was developed and recommended by Chaparala et al. [20] to understand the curing behaviour of any resin system prior running it in a pultrusion manufacturing line which will assist in determining the required line speed and temperature of heaters.

#### 4.2.1. Resin curing properties using DSC test

Fig. 4a shows the heat flow profile of the bisphenol-based epoxy under various ramp temperatures using the DSC instrument. It can be observed that increasing the heating ramp makes the reaction quicker to occur producing higher heat flow due to the increase in the reaction rate [22]. Thus, the time required to reach the peak reaction was plotted against the heating rate in Fig. 4b revealing consistent power-function relationship which means no effect of the heating rate on the reaction mechanism, as highlighted by Chaparala et al. [20].

#### 4.2.2. Resin curing properties using vacuum over trials

Vaccum oven trials were used to validate the DSC observations on large scale quantity of resin and to identify the critical temperature values for better understanding of the overall curing behaviour. Fig. 5a shows the development of the curing through the reduction of the resin viscosity until the reaction kick-off point, represented by the inflection point between the descending and ascending behaviours in the ion viscosity. At the same time, Fig. 5b shows the uniform heating of the resin in various rates against the isothermal oven temperature. It is noteworthy highlighting that the isothermal temperature reveals linear increase in the heating rate of the resin. This behavior indicates that no significant reaction occurred prior to the kick-off reaction point, as can be observed in Fig. 5c. This also assists in predicting the location where the kick-off reaction point will take place in the pultrusion manufacturing line, as described in later section. Furthermore, the increase in the heating rates resulted in earlier kick-off reaction time (see Fig. 5d) due to reaching the activation energy early to commence the polymerization. The relationship in Fig. 5d shows a similar trend (heat rate vs starts of kick-off reaction) as seen in Fig. 4b collected from the DSC test. This result adds a validity to this procedure to be used in characterising the polymerisation properties of the resin prior using it in the pultrusion manufacturing line.

When the resin reaches a specified temperature (126 C° as seen in Fig. 5b), regardless of the preset (ios-thermal) temperature of the oven, the initiators become activated. The first two stages of polymerization (initiation and propagation) then occurred as indicated by the increase in the ion-viscosity shown in Fig. 5a. This causes a spike in the heat exerted by the chemical reaction, which is seen as a peak in the temperature profile (Fig. 5b). Once the chemical reaction is completed, there is no further increase in temperature, which is the reason for the temperature drop after reaching the peak to reflect the set oven temperature. It should be mentioned that the sample cured at 100 C° reached 126 C° after a long time compared to the ones cured at 120, 150 and 180 C°. This is attributed to the accumulative energy absorbed by the resin to reach the activation energy of the initiators. This set temperature will not be suitable for dynamic pultrusion line as this manufacturing process has a time restraint, which is typically less than five minutes. The same observation was noticed by Chaparala et al. [20].

#### 4.2.3. Curing validation using commercial manufacturing putrusion line

The manufacturing trials of pultruding three GFRP bar diameters was achieved using a costume made metallic forming die with a length of 150 mm and 8 m long heating tunnel die with four heating zones (spaced at 2 m from each other) at various set temperatures (shown in Fig. 6) and with 450 mm by 160 mm internal cross-section. The pullers have three tonnes pulling capacity with maximum pulling speed of 5 m/min. The pull speed was set at 1.7 m/min for manufacturing all GFRP bar diameters. The set temperature and the pulling speed are pre-set as industrial practice at the commercial manufacturing facility of Beyond Materials Group Pty Ltd in Australia. Fig. 6 shows the temperature profile of the pultruded GFRP bars (10 mm, 12 mm, and 16 mm) in addition to a temperature profile of a sensor ran within a dry stack fibre to validate the internal temperature. A good matching between these temperature profiles was achieved. It should be highlighted that only thermocouples were able to be inserted at the middle of fibres as it was difficult to insert the DEA sensor due to its width (12 mm). Several attempts led to damage of the DEA sensors within the forming die and thread winding (see Fig. 3c and d). Nevertheless, the relationship between the thermocouple and the DEA sensors was already observed and known in the oven curing trials (Fig. 5a and b).

When the wet fibres enter the die, the temperature rises reflecting the heated tunnel die until reaching the kick-off reaction temperature. This is noticed around 126 C°, as observed in the oven trials (Fig. 5b). Various

**Table 3**
The newly designed GFRP bars.

| Bar size | Nominal dia. (mm) | Nominal area ($mm^2$) | Max. allowable area* ($mm^2$) | Max. allowable dia.* (mm) | Actual measured area ($mm^2$) | Actual measured dia. (mm) | Percentage increase in area (%) | Percentage increase in dia. (%) |
|---|---|---|---|---|---|---|---|---|
| **M10** | 9.5 | 70.9 | 104 | 11.51 | 91.9 | 10.82 | 29.7 % | 13.9 % |
| **M12** | 12.7 | 126.7 | 169 | 14.67 | 145.7 | 13.62 | 15.0 % | 7.2 % |
| **M16** | 15.9 | 198.6 | 251 | 17.88 | 221.7 | 16.80 | 11.7 % | 5.7 % |

* Based on ASTM D7957–22 specification.

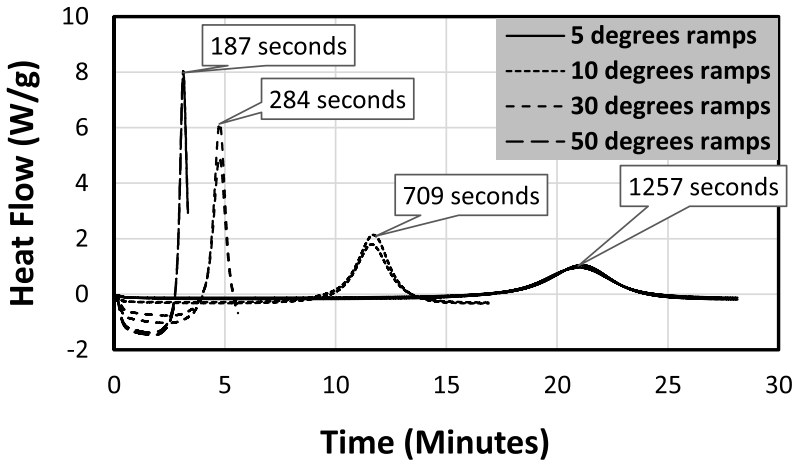


(a) Heat flow vs various ramp temperature

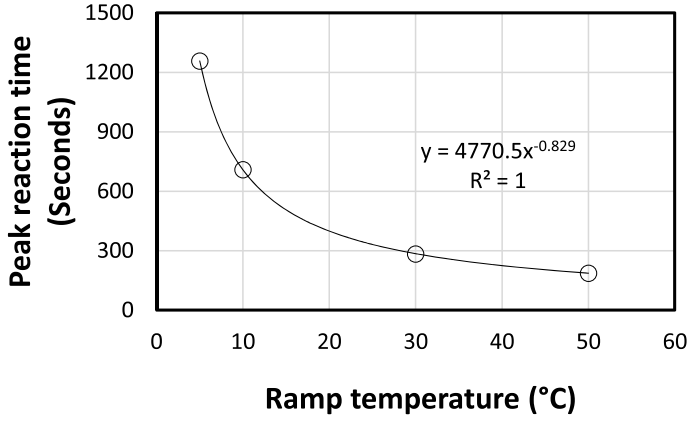


(b) Influence of ramp temperature on the peak reaction time

**Fig. 4.** Thermal properties and curing behaviour of the resin using DSC.

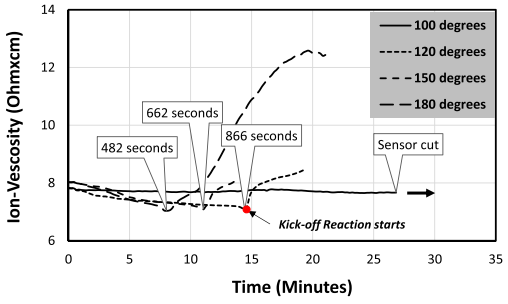


(a) Influence of ramp temperature on the peak reaction time

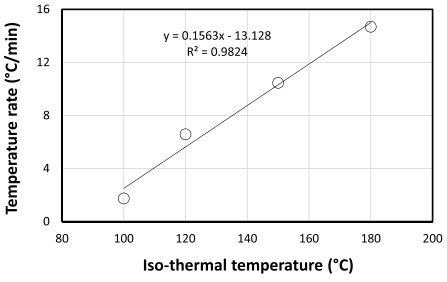


(c) Influence of the iso-thermal temperature on the temperature rate increase

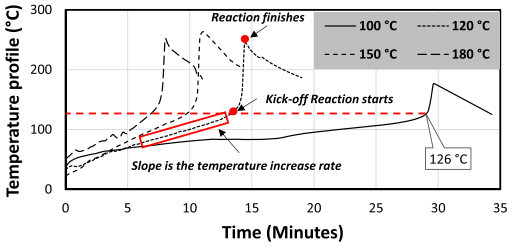


(b) Temperature profile of the tested specimens under various iso-thermal temperature

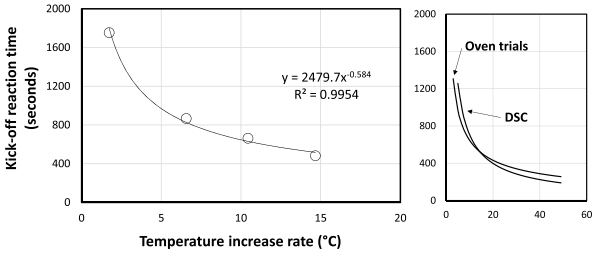


(d) Influence of iso-thermal oven temperature on the kick-off reaction time

**Fig. 5.** Thermal properties and curing behaviour of the resin using various isothermal oven conditions.

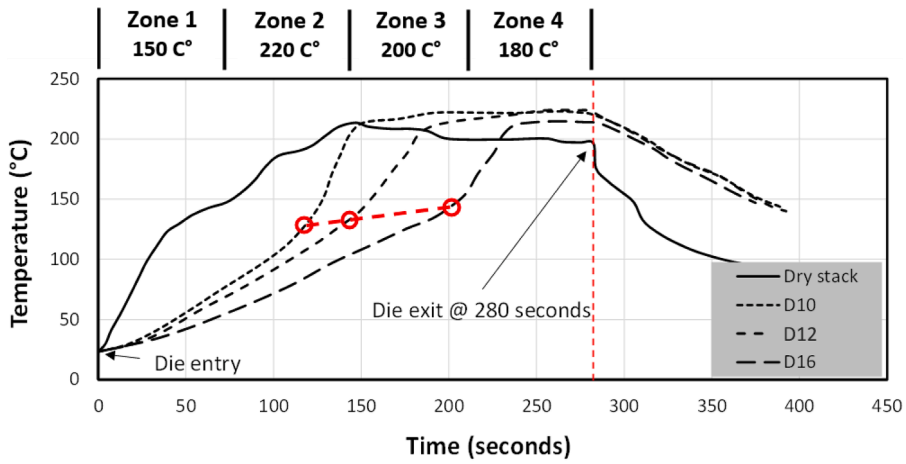


**Fig. 6.** Temperature profile of the pultruded GFRP bars.

heating rates can be observed in Fig. 6 due to the increase in the GFRP bar diameter (10 mm, 12 mm and 16 mm). Once the reaction kicked-off, high heat is exerted by the chemical reaction. This progresses until reaching the peak of exotherm in the temperature profile at the end of Zone 2 for the 10 mm bar, Mid of Zone 3 for 12 mm bar, and mid Zone 4 for the 16 mm bar. When the chemical reaction is complete, the temperature profile matches the heating tunnel die until getting out to drop the temperature in further reflecting the ambient temperature. It should be mentioned that understanding these observations allowed to run bigger bar diameters while ensuring fully cured conditions. It can also assist in accelerating the line speed of the selected bars to secure higher productivity.

### 4.3. *Cure kinetic predictions*

The DSC data considering various heating ramp temperatures (Fig. 4) were imported into the Netzsch Proteus Thermal Analysis software to predict the cure kinetics of the resin used in this study. This software can pick the best kinetic equation that expresses the curing behaviour for the used resin. Accordingly, the best fit thermo-kinetic equation was the reaction of $n^{th}$ order with autocatalysis (Cn) [23](as seen in Eq. (4)). In this equation, $d\alpha/dt$ is rate of cure with respect to time (*mol/litre.second*),

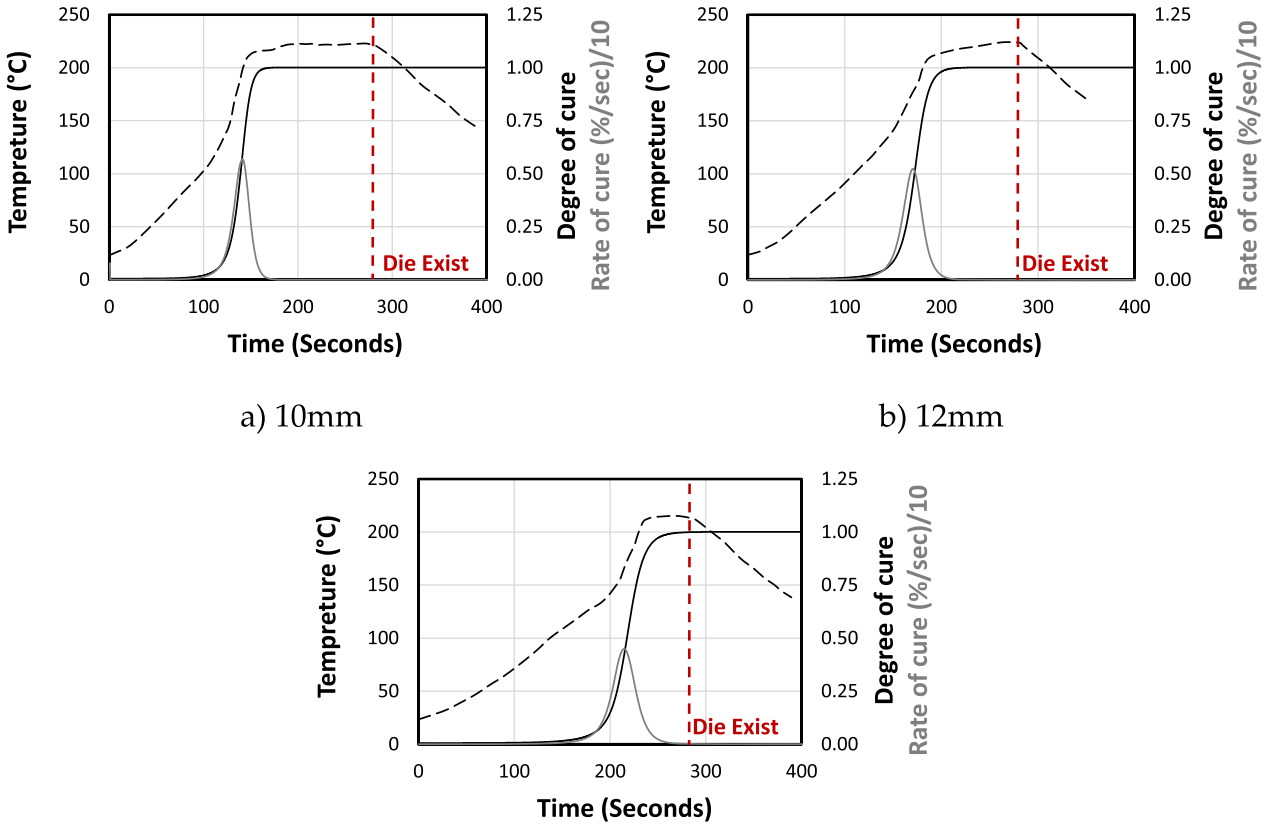


**Fig. 7.** Prediction of DC and RC of the manufactured GFRP bars.

k(T) represents the dependency of reaction rate on Temperature = $\left(Ae^{-E_a/RT}\right)$ (*mol/litre*), f(α) represents dependency of reaction rate on conversion = $(1-\alpha)^n$ (*mol/litre*), *A*= Pre exponential factor (6.35), $E_a$ = Activation energy (75.776) (*Joul/mol*), *R*= Gas constant (8.314) (*Joul/(mol.Kelvin)*), *T* = Time, *n*= Reaction order (1.35), $K_{cat}$ is the activation constant (1.66), and α = conversion.

$$\frac{d\alpha}{dt} = k(\mathrm{T}).\ \mathrm{f}(\alpha) = \left(Ae^{\frac{-E_a}{RT}}\right)(1+K_{cat}\alpha)(1-\alpha)^n \quad (4)$$

Fig. 7 shows rate of cure (RC) and the degree of cure (DC) of the manufactured GFRP bars with various bar diameters. In Fig. 7, based on the temperature profiles (Fig. 6), the prediction shows the evolution of the curing reaction through a significant increase in the RC achieved simultaneously when kicking off the reaction until obtaining a constant temperature just after the exothermic peak. Whereas the DC (the solid black line in Fig. 7) is developed also at the same time when the reaction got kicked off showing almost full curing (99.4 % for all manufactured bars) just after recording the maximum exothermic temperature. These results indicated full cure of the bar's core allowing to accelerate the line speed by shifting the curing to be prior to the end of the die or accommodate bigger GFRP bar diameters.

## 5. Material characterisation

In this section, the thermal, physical, and mechanical properties of the manufactured GFRP bars are presented validating the empirical design of these bars as calculated in previous sections.

### 5.1. Thermal properties

The transition glass temperature and the degree of cure were measured for the manufactured GFRP bars to validate the observations seen in the temperature profile. Figs. 5b, 6, and 7 show the maximum exotherm temperature indicates the highest possible degree of cure through the manufacturing process. According to the ASTM E2160–18 [24], the degree of cure (DC) of the 16 mm bar diameter (representing the possible least degree of cure due to its larger diameter) was 98.8 %. This is based on the DSC results of the cured and uncured resin. The glass transition temperature ($T_g$) of the cured GFRP bars was measured by DSC test as reported by Table 4. These results comply with the requirements of CSA S807–19, AS5204–23, and ACI 440R-22 in having a DSC and $T_g$ of higher than 95 % and 100 °C, respectively.

### 5.2. Physical properties

The designed cross-sectional area of the manufactured GFRP bars (Fig. 8) was checked in accordance with ASTM D7205 [25]. It is important to note that all five cuts of each bar size, as recommended by the specification, were immersed in water simultaneously to minimize errors in measuring the displaced water volume, which was used to determine the total volume of the bars. The total volume was then divided by five to calculate the average volume of each bar. As shown in Table 5, the average measured cross-sectional area of the manufactured GFRP bars was slightly larger than (around 3 %) the nominal diameter reported in Table 3. This discrepancy is attributed to the sand-coated layer applied to the outer surface, which serves to protect the bars and enhance their bond with the surrounding concrete in structural applications. Table 5 also shows the fibre content and the fibre volume fraction of the manufactured and tested GFRP bars, as per the burn out test in accordance with ASTM D570–10 [26]. Moreover, five specimens were cut into a length of 25 mm using diamond saw. Afterwards, the specimens were polished (300, 600 and 1200 grids) and observed under the microscope to see the voids inside the bars and compared to the surface area of the bar (see Table 5). Noting that the void ratio is calculated by dividing the surface area of the observed voids (the accounted voids are the macro voids having dimensions bigger than 50 μm) by the surface area of the bar. This approach was conducted by Vedernikov et al. [27] to measure the void ratio accurately. On the other hand, as worst-case scenario, three 50 mm long specimens of 10 mm bar diameter were sealed by resin at the edges and soaked in water at room temperature for seven days (168 hrs) at 50 °C, where their weight was taken at 24 hrs and 72 hrs and 168 hrs. In addition, transverse coefficient of thermal expansion (TCTE) test was conducted to see the lateral expansion of the manufactured bar under ramp temperature from −30 °C to 60 °C at a heating rate of 3 °C. Similar to the degree of cure, a 16 mm bar diameter was chosen to evaluate the void ratio and TCTE, as it represents the highest likelihood of defect occurrence with increasing bar size [28,29]. The results are shown in Table 5. These test results show compliance to the requirements highlighted by ASTM D7957–22 [15] for solid round glass fiber reinforced polymer bars.

**Table 4**
Glass transition temperature and degree of cure of the tested GFRP bars.

| Specimen | $T_g$ (°C) | DC (%) |
|---|---|---|
| 1 | 127.8 | 99.1 |
| 2 | 125.4 | 98.5 |
| 3 | 128.6 | – |
| Average (MPa) | **127.3** | **98.8** |
| St. D. (MPa) | **1.4** | **0.3** |
| CoV (%) | **1.1** | **0.3** |

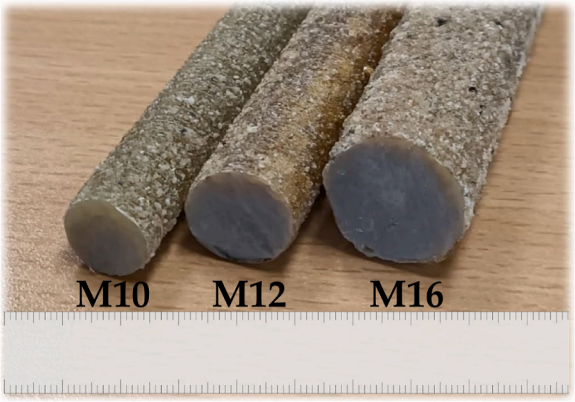


**Fig. 8.** cross-section of the newly manufactured GFRP bars.

### 5.3. Mechanical properties

Tensile, interlaminar shear strength (ILSS), and transverse shear (TS) tests were conducted to characterise the mechanical properties of the manufactured GFRP bars. Five GFRP bars of each bar diameter were prepared and tested in tension, ILSS and TS in accordance with ASTM D7205–16 [25], ASTM D4475–21 [30], and ASTM D7617–17 [31], respectively. Test setup for the mechanical tests is shown in Fig. 9. The table shows the tensile failure load, strength (based on the nominal diameter), and elastic modulus of the tested GFRP bars. It can be noticed that all bars achieved an elastic modulus higher than 60 GPa based on the nominal bar diameter (noted for Grade III GFRP bars based on CSA S807 [14] and E60 based on AS5204 [17]). It is also noted that the increase in the bar diameter resulted in a reduction in the tensile strength and modulus (see Table 6). This is attributed to the limit ability to achieve the same actual-to-nominal bar diameter for different bar sizes, as mentioned in Section 4.1.2. Moreover, high stresses in the smaller-diameter bars are attributed to the shear-lag effects [32,33].

In comparison to the design modulus of elasticity (Eq. (1)), it can be noted that the tested GFRP bars achieved remarkably close values to the designed one within an error of 7 % for M10 and 2 % for M12 and M16. However, the designed strength (Eq. (2)) was 40–50 % higher than the

**Table 5**
Physical properties of the tested bars.

| Specimen | Cross-sectional area($mm^2$) | | | Fibre volume fraction (%) | | | Void ratio (%) | Water absorption(@24 hrs) | Water absorption(@saturation-168 hrs) | TCTE $\times 10^{-6}$/°C |
|---|---|---|---|---|---|---|---|---|---|---|
| | 10 mm | 12 mm | 16 mm | 10 mm | 12 mm | 16 mm | 16 mm | 16 mm | 16 mm | 16 mm |
| 1 | – | – | – | 66.4 % | 65.4 % | 63.5 % | 0.12 % | 0.13 % | 0.17 % | 18.2 |
| 2 | – | – | – | 66.3 % | 66.8 % | 63.7 % | 0.00 % | 0.13 % | 0.18 % | 22.1 |
| 3 | – | – | – | 65.9 % | 65.4 % | 63.3 % | 0.00 % | 0.15 % | 0.17 % | 22.9 |
| 4 | – | – | – | – | – | – | 0.19 % | – | – | – |
| 5 | – | – | – | – | – | – | 0.08 % | – | – | – |
| Average | **94.3** | **150.8** | **228.1** | **66.2** | **65.9** | **63.5** | **0.078 %** | **0.14 %** | **0.18 %** | **21.07** |
| St. D. | – | – | – | 0.23 | 0.64 | 0.17 | – | 0.01 | 0.00 | 2.05 |
| CoV (%) | – | – | – | 0.34 | 0.97 | 0.26 | – | 6.0 | 1.5 | 9.7 |

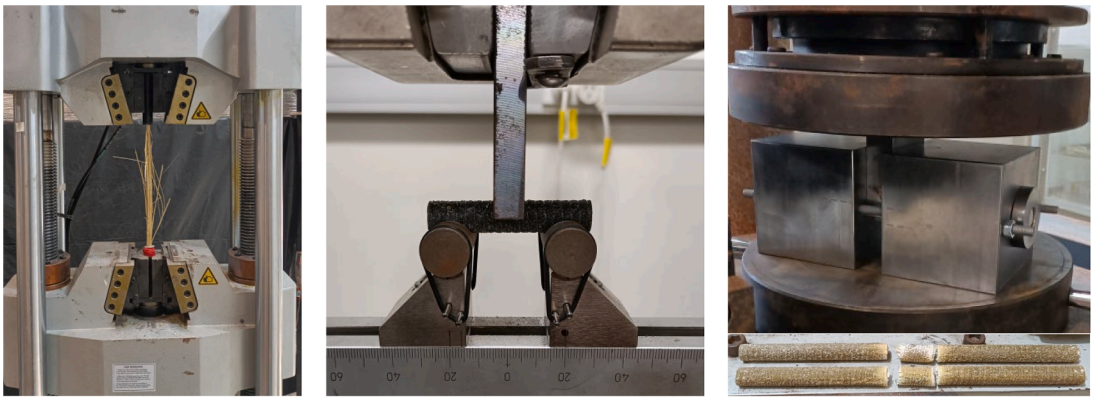

(a) Tensile (b) ILSS (c) TS

**Fig. 9.** Test setup.

**Table 6**
Tensile results of the tested bars.

| Specimen | 10 mm | | | 12 mm | | | 16 mm | | |
|---|---|---|---|---|---|---|---|---|---|
| | Failure load (kN) | Ultimate Stress | Elastic Modulus | Failure load (kN) | Ultimate Stress | Elastic Modulus | Failure load (kN) | Ultimate Stress | Elastic Modulus |
| | | (MPa) | (GPa) | | (MPa) | (GPa) | | (MPa) | (GPa) |
| 1 | 105.9 | 1492 | 68.3 | 163.8 | 1289.9 | 62.5 | 239.2 | 1202 | 65.0 |
| 2 | 104.8 | 1476 | 68.3 | 167.1 | 1315.6 | 62.5 | 234.7 | 1179 | 62.9 |
| 3 | 97.05 | 1367 | 67.9 | 168.5 | 1327.0 | 63.8 | 243.9 | 1226 | 60.9 |
| 4 | 99.95 | 1408 | 66.3 | 164.9 | 1298.2 | 62.8 | 239.1 | 1202 | 60.4 |
| 5 | 96.80 | 1363 | 66.9 | 162.0 | 1275.7 | 63.3 | 229.7 | 1154 | 59.1 |
| Average | – | **1421** | **68.3** | – | **1301** | **62.98** | – | **1193** | **61.66** |
| SD (MPa) | – | **53.7** | **0.8** | – | **18.2** | **0.54** | – | **24.1** | **2.34** |
| CoV (%) | – | **3.8** | **1.1** | – | **1.4** | **0.9** | – | **2.0** | **3.8** |

strength achieved by the tested GFRP bars. This is attributed to the complicated failure mechanisms in composites which involve several parameters not accounted in the design strength equation including presence of voids, misalignment, shear strength between fibres, and interfacial bond between the matrix and filaments [34,35].

The ILSS of the smaller-diameter bars was higher than the larger-diameter bars (Table 7) due to the uniformity of stress distribution across smaller specimen cross sections than across larger ones. This finding agrees with Benmokrane et al. [33] for the tested 13 mm and 15 mm GFRP bar diameters. For the same reason, TS in Table 8 was noticed to be higher at smaller bar diameter compared to the larger ones.

**Table 7**
ILSS results of the tested bars.

| Specimen | 10 mm | | 12 mm | | 16 mm | |
|---|---|---|---|---|---|---|
| | Failure load(N) | ILSS (MPa) | Failure load(N) | ILSS (MPa) | Failure load(N) | ILSS (MPa) |
| 1 | 7768 | 82.2 | 12,874 | 76.2 | 15,901 | 60.1 |
| 2 | 7964 | 84.3 | 12,693 | 75.1 | 15,875 | 60.0 |
| 3 | 8135 | 86.1 | 13,294 | 78.7 | 14,407 | 54.4 |
| 4 | 8401 | 88.9 | 12,616 | 74.7 | 15,404 | 58.2 |
| 5 | 8317 | 88.0 | 12,452 | 73.7 | 14,840 | 56.1 |
| Average | | **85.9** | | **75.7** | | **57.8** |
| SD (MPa) | | **2.4** | | **1.7** | | **2.2** |
| CoV (%) | | **2.8** | | **2.3** | | **3.8** |

## 6. Conclusions

This manuscript examines the current practice of designing GFRP

**Table 8**
TS strength results of the tested bars.

| Specimen | 10 mm | | 12 mm | | 16 mm | |
|---|---|---|---|---|---|---|
| | Failure load(kN) | TS (MPa) | Failure load(kN) | TS (MPa) | Failure load(kN) | TS (MPa) |
| 1 | 40.65 | 286.8 | 72.27 | 285.2 | 80.59 | 203.0 |
| 2 | 43.55 | 307.2 | 75.11 | 296.4 | 89.08 | 224.4 |
| 3 | 41.31 | 291.4 | 74.32 | 293.3 | 84.57 | 213.0 |
| 4 | 42.79 | 301.8 | 72.92 | 287.8 | 93.26 | 234.9 |
| 5 | 42.36 | 298.8 | 71.16 | 280.8 | 91.45 | 230.4 |
| Average | | **297.2** | | **288.7** | | **221.1** |
| SD (MPa) | | **7.3** | | **5.6** | | **11.7** |
| CoV (%) | | **2.5** | | **1.9** | | **5.3** |

bars and the influencing parameters contributing to the design of a range of selected diameters. It outlines the crucial manufacturing variables involved in the pultrusion process and offers a practical example of a step-by-step design and production method for new GFRP bars, utilising both theoretical and experimental approaches. This study provides valuable guidance for GFRP manufacturers, enabling them to identify the key parameters that influence the production of high modulus GFRP bars as internal reinforcement in concrete structures. Conclusions from this study can be summarised as follows:

- CSA S807 shows better consistency in the design of the bar diameter compared to the ASTM D7957 specification. In the former, the margin between the actual and nominal bar diameter allows to achieve high elastic modulus GFRP bars in systematic approach.
- Designing high performing GFRP bars depends on understanding the mix design of the fibre-to-resin ratio and using the preliminary theoretical principles to achieve certain amount of fibre content in a selected bar size. This allows designing a compatible forming die of the selected GFRP bar size.
- Prior manufacturing, resin should go through thermal testing (DSC and vacuum oven trials) to understand its curing behaviour and decide accordingly the temperature set required to complete the curing reaction within the curing die in the pultrusion manufacturing line.
- Achieving the required degree of cure with taking care of the critical manufacturing parameters as well as required geometry will result in acceptable physical and mechanical properties of GFRP bars that can be utilised as internal reinforcements in concrete structures.

It is recommended for further research considering higher fibre volume fraction bars is conducted to obtain new GFRP bars with higher modulus than the ones existed in the market. This will also allow better understanding of how this increase affects other properties with more caution regarding the manufacturing process.

## CRediT authorship contribution statement

**Omar Alajarmeh:** Writing – original draft, Validation, Resources, Project administration, Methodology, Investigation, Formal analysis, Data curation, Conceptualization. **Allan Manalo:** Writing – review & editing, Supervision, Investigation. **Dmitry Yatsenko:** Writing – review & editing, Resources, Methodology, Funding acquisition.

## Declaration of competing interest

The authors would like to declare and confirm that there is no conflict of interest of this manuscript.

## Acknowledgements

The authors are grateful for the assistance of the technicians at the Centre of Future Materials (CFM). The authors also like to thank Beyond Materials Group (BlackBar) Australia for utilising their facility to pultrude the GFRP bars and conducting this research work. The 1st author wishes to acknowledge the financial support of the Advance Queensland Industry Research Fellowship Program (AQIRF 128–2021) to complete this research work.

## Data availability

Data will be made available on request.

## References

[1] Ahmed El-Nemr, El-Safty, Benmokrane, Evaluation of the flexural strength and serviceability of concrete beams reinforced with different types of GFRP bars, Eng. Struct. 173 (2018) 606–619.
[2] Manalo Maranan, Karunasena Benmokrane, Mendis, Nguyen, Flexural behavior of geopolymer-concrete beams longitudinally reinforced with GFRP and steel hybrid reinforcements, Eng. Struct. 182 (2019) 141–152.
[3] Yang Ebrahimzadeh, Alajarmeh Manalo, Sorbello Senselova, Weerakoon, Benmokrane, Flexural behaviour of GFRP-reinforced concrete pontoon decks under static four-point and uniform loads. Structures, Elsevier, 2024.
[4] Manalo AlAjarmeh, Karunasena Benmokrane, Mendis, Nguyen, Compressive behavior of axially loaded circular hollow concrete columns reinforced with GFRP bars and spirals, Constr. Build. Mater. 194 (2019) 12–23.
[5] Manalo AlAjarmeh, Karunasena Benmokrane, Mendis, Axial performance of hollow concrete columns reinforced with GFRP composite bars with different reinforcement ratios, Compos. Struct. 213 (1) (2019) 12.
[6] Manalo AlAjarmeh, Karunasena Benmokrane, Mendis, Effect of spiral spacing and concrete strength on behavior of GFRP-reinforced hollow concrete columns, J. Compos. Const. 24 (1) (2019) 04019054.
[7] Alajarmeh Manalo, Sorbello Cooper, Weerakoon, Benmokrane, Manufacturing and structural performance of glass-fiber-reinforced precast-concrete boat ramp planks. Structures, Elsevier, 2020.
[8] Alajarmeh Manalo, Ferdous Yang, Benmokrane Ebrahimzadeh, Weerakoon Sorbello, Lutze, Development and mechanical performance evaluation of a GFRP-reinforced concrete boat-approach slab. Structures, Elsevier, 2022.
[9] Tardif Nawab, Sobotka Boyard, Casari, Jacquemin, Determination and modelling of the cure shrinkage of epoxy vinylester resin and associated composites by considering thermal gradients, Compos. Sci. Technol. 73 (2012) 81–87.
[10] Cavalcante Schneider, Silikas, Shrinkage stresses generated during resin-composite applications: a review, J. Dent. Biomech. 2010 (2009) 131630.
[11] Wang Derradji, Liu, Phthalonitrile Resins and Composites, William Andrew Publishing, 2018, pp. 107–174.
[12] Höfer Pascault, Fuertes, Polymers for a sustainable environment and green energy, Polym. Sci.: Comprehen. Ref. (2012) 59.
[13] ISIS Design Manual, Reinforced Concrete Structures With Fibre-Reinforced Polymers, ISIS Canada Research Network. Winnipeg, MB: University of Manitoba, 2007, p. 151.
[14] S807-10, Specification For Fibre Reinforced Polymers, Rexdale, Ontario, Canada, 2010.
[15] D7957M-22, Standard Specification for Solid Round Glass Fiber Reinforced Polymer Bars for Concrete Reinforcement, ASTM International, West Conshohocken, PA, 2022.
[16] Mendis Manalo, Jachmann Bai, Sorbello, Fiber-reinforced polymer bars for concrete structures: state-of-the-practice in Australia, J. Compos. Const. 25 (1) (2021) 05020007.
[17] 5204:2023, Australian standard for fibre-reinforced polymer bars 2023.
[18] CSA S806, Design and construction of building structures with fibre-reinforced polymers. 2012: Canadian Standards Association, CAN/CSA-S806-12, Rexdale, ON, Canada.
[19] ACI-440.11-22, Building Code Requirements For Structural Concrete Reinforced with Glass Fiber-Reinforced Polymer (GFRP) Bars—Code and Commentary. American Concrete Institute, USA, 2022.
[20] Alajarmeh Chaparala, Zeng Shelley, Voice Rendle-Short, Schubel, Characterisation of curing of vinyl ester resin in an industrial pultrusion process: influence of die temperature, Polymers (Basel) 15 (18) (2023) 3808.
[21] Alajarmeh Qi, Shelley Alhawamdeh, Rendle-Short Schubel, Zeng, Formation of non-uniform fibre distribution and its effect on the flexural performance of pultruded GFRP box beams, Compos. Struct. 327 (2024) 117695.
[22] Karkanas, Partridge, Cure modeling and monitoring of epoxy/amine resin systems. I. Cure kinetics modeling, J. Appl. Polym. Sci. 77 (7) (2000) 1419–1431.
[23] Nasonov Vedernikov, Gusev Korotkov, Akhatov, Safonov, Effects of additives on the cure kinetics of vinyl ester pultrusion resins, J. Compos. Mater. 55 (21) (2021) 2921–2937.
[24] E2160, Standard test method for heat of reaction of thermally reactive materials by differential scanning calorimetry. American Society for Testing and Materials West Conshohocken, PA, 2018.
[25] ASTM D7205/D7205M-16, Standard Test Method For Tensile Properties of Fiber Reinforced Polymer Matrix Composite Bars, ASTM International, West Conshohocken, PA, 2016.

[26] ASTM D570-10, Standard Test Method For Water Absorption of Plastics, ASTM, West Conshohocken, PA, USA, 2010.
[27] Minchenkov Vedernikov, Sulimov Gusev, Li Zhou, Akhatov Xian, Safonov, Effects of the pre-consolidated materials manufacturing method on the mechanical properties of pultruded thermoplastic composites, Polymers (Basel) 14 (11) (2022) 2246.
[28] Manalo Benmokrane, Mohamed Bouhet, Robert, Effects of diameter on the durability of glass fiber–reinforced polymer bars conditioned in alkaline solution, J. Compos. Const. 21 (5) (2017) 04017040.
[29] Alajarmeh Qi, Schubel Shelley, Rendle-Short, Zeng, Fibre waviness characterisation and modelling by filtered canny misalignment analysis (FCMA), Compos. Struct. 307 (2023) 116666.
[30] ASTM D4475-21, Standard Test Method For Apparent Horizontal Shear Strength of Pultruded Reinforced Plastic Rods By the Short-Beam Method, ASTM International, West Conshohocken, PA, 2021.
[31] ASTM D7617-17, Transverse Shear Equipment For Polymer Matrix Composites, ASTM International, West Conshohocken, PA, 2017.
[32] Wu, Thermomechanical Properties of Fiber-Reinforced Plastic (FRP) Bars, West Virginia University, 1991.
[33] Hassan Benmokrane, Vijay Robert, Manalo, Effect of different constituent fiber, resin, and sizing combinations on alkaline resistance of basalt, carbon, and glass FRP bars, J. Compos. Const. 24 (3) (2020) 04020010.
[34] Fragoudakis, Strengths and limitations of traditional theoretical approaches to FRP laminate design against failure, Eng. Fail. Anal. (2020) 3.
[35] Li Li, Deng Shao, Ma Kou, Zhang Zhang, Chen, Qu, Modeling the effects of interfacial properties on the temperature dependent tensile strength of fiber reinforced polymer composites, Compos. Sci. Technol. 172 (2019) 74–80.